Diffusion-controlled generation of a proton-motive force across a biomembrane

Anatoly Yu. Smirnov,[1,2] Sergey E. Savel'ev,[1,3] and Franco Nori[1,2]
[1]*Advanced Science Institute, The Institute of Physical and Chemical Research (RIKEN), Wako-shi, Saitama 351-0198, Japan*
[2]*Center for Theoretical Physics, Department of Physics, The University of Michigan, Ann Arbor, Michigan 48109-1040, USA*
[3]*Department of Physics, Loughborough University, Loughborough LE11 3TU, United Kingdom*
(Received 6 May 2009; published 22 July 2009)

Respiration in bacteria involves a sequence of energetically coupled electron and proton transfers creating an electrochemical gradient of protons (a proton-motive force) across the inner bacterial membrane. With a simple kinetic model, we analyze a redox loop mechanism of proton-motive force generation mediated by a molecular shuttle diffusing inside the membrane. This model, which includes six electron-binding and two proton-binding sites, reflects the main features of nitrate respiration in *E. coli* bacteria. We describe the time evolution of the proton translocation process. We find that the electron-proton electrostatic coupling on the shuttle plays a significant role in the process of energy conversion between electron and proton components. We determine the conditions where the redox loop mechanism is able to translocate protons against the transmembrane voltage gradient above 200 mV with a thermodynamic efficiency of about 37%, in the physiologically important range of temperatures from 250 to 350 K.

DOI: 10.1103/PhysRevE.80.011916 PACS number(s): 87.16.A−, 87.16.Uv, 73.63.−b

I. INTRODUCTION

Diffusion-controlled electron and proton transfer reactions are pivotal for the efficient energy transformation in respiratory chains of animal cells and bacteria. During the process of respiration the energy extracted from sunlight or from food molecules is converted into an electrochemical gradient of protons (also called a proton-motive force) across an inner mitochondrial or bacterial membrane [1–4]. Thereafter, this energy is harnessed by adenosine triphosphate (ATP) synthase for a synthesis of ATP molecules, the main energy currency of the cell. The energy stored in the proton gradient can be also used to drive a rotation of a bacterial flagellar motor.

The energetically uphill translocation of protons is accomplished by a set of membrane-embedded proton pumps or by a redox loop mechanism proposed in the original formulation of chemiosmotic theory [5]. For a true proton pump (e.g., cytochrome *c* oxidase), electrogenic events are associated with charges of protons crossing the membrane [2,3]. In the redox loop mechanism, the transmembrane voltage is generated by electron charges moving across the membrane. This mechanism is responsible for a proton-motive force generation in the respiratory chain of anaerobically grown bacteria such as the facultative anaerobe *Escherichia coli*. In the absence of oxygen and in the presence of nitrate, *E. coli* can switch from oxidative respiration, which uses oxygen molecules as terminal electron acceptors, to nitrate respiration, where nitrogen plays the role of a terminal acceptor of electrons in the process of nitrate-to-nitrite reduction.

The redox loop is formed by the formate-dehydrogenase-N (Fdh-N) enzyme and by the nitrate reductase enzyme (Nar) (Fig. 1). The structures of these enzymes and positions of all redox centers have recently been determined [6–9]. As a result of formate reduction $HCOO^- \rightarrow CO_2 + H^+ + 2e^-$, a pair of high-energy electrons is delivered to the beginning of the pathway (source S) at the P side of the inner (or plasma) membrane of *E. coli*. Through the intermediate iron-sulfur clusters electrons are transferred, one after another, to the integral membrane subunit of Fdh-N, which includes hemes b_P (site 1) and b_C (site 2) located on the opposite sides of the membrane (see Fig. 1). The subindices *P* and *C* here refer to "periplasm" and "cytoplasm," respectively.

E. coli utilizes a molecule of menaquinone (MQ) as a movable shuttle connecting the Fdh-N and Nar enzymes. Near the N side of the membrane, menaquinone is populated with two electrons donated by heme b_C. In this process, menaquinone accepts two protons from the N side of the membrane turning into the form of menaquinol (MQH_2). The neutral menaquinol molecule diffuses to the P side where it donates two electrons to heme b_L of the nitrate reductase and, simultaneously, two protons to the P-side proton reservoir.

Electrons are transferred, one by one, through heme b_L (site 5), to heme b_H (site 6) and, subsequently, through several iron-sulfur clusters, to the site D on the cytoplasmic (N) space where the electrons reduce nitrate to nitrite $NO_3^- \rightarrow NO_2^- + H_2O$. The *L* and *H* subindices in the notations b_L and b_H for the sites 5 and 6 refer to "low" and "high" redox potentials, respectively. Note that at the beginning of the electron-transport chain (ETC), where the formate is oxidized to CO_2 and H^+, the midpoint redox potential is very low $E_m = -420$ mV. Thus, electrons entering ETC have high energies (~420 meV). The menaquinone/menaquinol pair MQ/MQH_2 has a much higher redox potential $E_m = -80$ mV (and energy on the order of +80 meV), which makes possible the electron translocation against the transmembrane voltage. In the second half of the redox loop formed by nitrate reductase, electrons also move energetically downhill from quinol ($E_m = -80$ mV) to the nitrate reduction site having a midpoint potential $E_m \sim +420$ mV (and energy ~−420 meV) [10].

A geometrical disposition of the quinone-reducing center b_C and the quinol-oxidizing center b_L on opposite sites of the membrane is crucial for the generation of the proton-motive

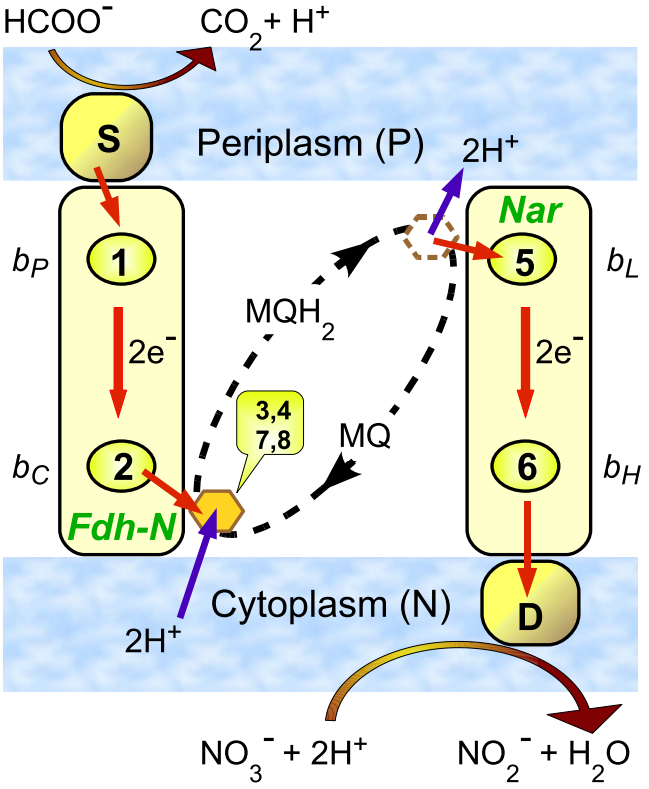

FIG. 1. (Color online) Schematic diagram of the redox loop. High-energy electrons are delivered from the source S to a redox center 1 (heme b_P) located near the periplasmic (P) side of the membrane. After that, electrons are transferred across the membrane to a redox site 2 (heme b_C) on the cytoplasmic (N) side. At the N side, two electrons reduce a molecule of menaquinone MQ, which also takes two protons from the N side turning into a molecule of menaquinol MQH_2. The menaquinone shuttle has two electron-binding sites 3 and 4 and two protonable sites 7 and 8. The neutral quinol molecule MQH_2 diffuses freely to the P side of the membrane, where its electron cargo is transferred to the redox site 5 (heme b_L), and, via the center 6 (heme b_H), to the drain D on the cytoplasmic side. The oxidation of the quinol molecule MQH_2 by the center 5 is accompanied by a release of two protons to the P side of the membrane. Formate-dehydrogenase (Fdh-N, with centers b_P and b_C) reduces the quinone molecule MQ. Nitrate reductase (Nar, with centers b_L and b_H) oxidizes the quinol molecule MQH_2. Both of these (Fdh-N and Nar) form the redox loop, generating a proton-motive force across the membrane.

force [3,6,7]. Electrogenic events resulting in the net charge translocation occur when an electron moves from heme b_P to heme b_C in the Fdh-N enzyme and from heme b_L to heme b_H located on the Nar enzyme.

The crystal structures of the Fdh-N and Nar enzymes solved in Refs. [6,7] provide key components for understanding the mechanism of proton-motive force generation through the redox loop. It should be emphasized, however, that the proton-motive force generation is a dynamical process, so that the structural analysis should be complemented by kinetic studies. For example, real time investigations of electron and proton transfers in complex I [11] and complex IV [12] of mitochondria allow elucidation of a time sequence of transfer events and get important information about electron and proton transition rates. Kinetic models of the proton pumping processes in cytochrome *c* oxidase [13,14] and in bacteriorhodopsin [15] are also proven to be beneficial for understanding experimental findings, as well as for an initiation of new experiments, giving a comprehensive picture of the phenomenon.

In the present work, we investigate a redox loop mechanism of a proton-motive force generation across the inner membrane of *E. coli* bacterium within a simple physical model incorporating two hemes b_P and b_C, in the Fdh-N enzyme, two hemes, b_L and b_H, in the Nar enzyme, and a molecular shuttle (menaquinone) diffusing between these two halves of the redox loop. This diffusion is governed by a Langevin equation. There is a pool of menaquinone/menaquinol molecules in the bacterial plasma membrane [2–4], but we only consider the contribution of a single menaquinone molecule to the electron and proton translocation processes. Because of this, the actual values of the electron and proton fluxes should be higher than the values calculated below. In order to describe the process of loading/unloading the shuttle with electrons and protons, we employ a system of master equations, with position-dependent transition rates between the shuttle and electron/proton reservoirs. With these equations, we analyze the time dependence of the proton-motive force generation process together with the dependence of numbers of transferred electrons and protons on a transmembrane voltage and on temperature. A thermodynamic efficiency of the proton translocation across the inner bacterial membrane is defined and calculated as well.

The paper is organized as follows. In Sec. II we introduce a model of the system and present a set of master and Langevin equations, which govern the time evolution of a proton translocation process. Section III is devoted to a discussion of the key parameters of the model. In Sec. IV we report our main results and describe the steps for the kinetics of electron and proton transfer steps. The conclusions of the paper are presented in Sec. V.

II. MODEL

We take into consideration (see Fig. 1) six sites for an electron pathway through the system: two sites 1 and 2, corresponding to hemes b_P and b_C of the Fdh-N enzyme; two electron-binding sites 3 and 4, on the menaquinone shuttle; and two sites 5 and 6 related to hemes b_L and b_H on Nar. For the sake of simplicity, we assume that heme b_P (site 1) located on the periplasmic (P) side of the membrane is coupled to the source of electrons S and that heme b_H (site 6) having a high midpoint potential is coupled to the electron drain D.

The source reservoir S characterized by an electrochemical potential μ_S and the drain reservoir D described by an electrochemical potential μ_D provide a continuous flow of electrons through the ETC. The potential μ_S roughly corresponds to the energy of electrons injected into the ETC after formate oxidation $\mu_S \sim 420$ meV, whereas the drain potential μ_D is related to the electron energy on the nitrate reduction site $\mu_D \sim -400$ meV. Note that we include the sign of the electron charge in the definition of the electron electrochemical potential. This means that a site with a higher elec-

tron energy is characterized by a more negative redox midpoint potential E_m. Here, all energy parameters are measured in meV.

Taking into account two (instead of one) redox sites 1 and 2 located on opposite sides of the membrane allows us to describe the process of transmembrane voltage generation during electron transfer along the Fdh-N complex. Additional transmembrane voltage is generated when an electron moves between two Nar sites 5 and 6, which are also located on the opposite sides of the membrane.

The pathway for protons includes two proton-binding sites 7 and 8 on the shuttle. We assume that the molecular shuttle moves along a line connecting the redox sites 2 and 5. Depending on the position of the shuttle x along this line, the proton-binding sites can be coupled either to the positive or to the negative sides of the membrane (P-and N-proton reservoirs). The distributions of protons in the P and N reservoirs are presumably described by the Fermi functions with the electrochemical potentials μ_P (P side) and μ_N (N side of the membrane). In its completely reduced form of menaquinol MQH_2, the shuttle has a maximum load of two electrons and two protons, whereas in its oxidized quinone form (denoted by MQ in Fig. 1) the shuttle is empty.

A. Hamiltonian of the electron-proton system

Within a formalism of secondary quantization [16–20], we introduce the creation and annihilation Fermi operators $a_\alpha^\dagger, a_\alpha$ for an electron located on the site α ($\alpha=1,\ldots,6$), as well as the corresponding Fermi operators $b_\beta^\dagger, b_\beta$ for a proton on the protonable site β ($\beta=7,8$). The electron population of the α site is described by the operator $n_\alpha=a_\alpha^\dagger a_\alpha$, whereas the proton population of the β site has the form $n_\beta=b_\beta^\dagger b_\beta$. Note that we use here methods of quantum transport theory to derive classical master equations. A similar approach has been applied in studies of quantum coherence in biological systems [21].

The main part of the system Hamiltonian H_0 involves contributions from the energies ε_α of electron sites and energies ε_β of two proton-binding sites on the shuttle complemented by terms describing electrostatic repulsions between sites 1 and 2 (with Coulomb energy u_{12}) and between sites 5 and 6 (with energy u_{56}). We also add an electron-electron Coulomb repulsion between two electron-binding sites 3 and 4 on the shuttle (with an energy scale u_{34}) and a term describing a repulsion between two protons on the sites 7 and 8, occupying the shuttle (energy u_{78}). An electrostatic attraction between electrons and protons traveling together on the menaquinol shuttle is described by the energy parameters u_{37}, u_{38}, u_{47}, and u_{48}. As a result, the basic Hamiltonian H_0 of the electron-proton system has the form

$$H_0=\sum_{\alpha=1}^{6}\varepsilon_\alpha n_\alpha+\sum_{\beta=7}^{8}\varepsilon_\beta n_\beta+u_{12}n_1n_2+u_{34}n_3n_4+u_{56}n_5n_6+u_{78}n_7n_8-u_{37}n_3n_7-u_{38}n_3n_8-u_{47}n_4n_7-u_{48}n_4n_8+(n_3+n_4-n_7-n_8)^2U_s(x). \quad (1)$$

The last term in Eq. (1), which depends on the shuttle position x, describes the contribution of a potential barrier $U_s(x)$, which prevents a charged shuttle from crossing the interior of the lipid membrane. The barrier has an almost rectangular shape,

$$U_s(x)=U_{s0}\left\{\left[\exp\left(\frac{x-x_s}{l_s}\right)+1\right]^{-1}-\left[\exp\left(\frac{x+x_s}{l_s}\right)+1\right]^{-1}\right\}, \quad (2)$$

with a height U_{s0}, a steepness l_s, and a width $2x_s$. This is multiplied by the shuttle charge squared $(n_3+n_4-n_7-n_8)^2$. The height U_{s0} of this potential is roughly equal to the energy penalty (in meV) for moving a molecule with a charge q_0 (in units of $|e|$) and a radius r_0 (in nm) from a medium with a dielectric constant ϵ_1 to a medium with a constant ϵ_2 [22],

$$U_{s0}=\frac{1440q_0^2}{2r_0}\left(\frac{1}{\epsilon_2}-\frac{1}{\epsilon_1}\right). \quad (3)$$

For example, the transfer of a charged molecule ($q_0=1$) with radius $r_0=0.3$ nm, from water ($\epsilon_1=80$) to the lipid membrane with $\epsilon_2=3$, results in the dielectric penalty $U_{s0}=770$ meV. The specific shape of the barrier $U_s(x)$ in Eq. (2) is of little importance for the results from this model.

Electrons in the source (drain) reservoir are described by the creation and annihilation operators $c_{k\mathrm{S}}^\dagger, c_{k\mathrm{S}}$ ($c_{k\mathrm{D}}^\dagger, c_{k\mathrm{D}}$) and for protons in the N (P) reservoir, we introduce operators $d_{q\mathrm{N}}^\dagger, d_{q\mathrm{N}}$ ($d_{q\mathrm{P}}^\dagger, d_{q\mathrm{P}}$), so that the Hamiltonian of the electron source and drain reservoirs H_{SD}, and the Hamiltonian of the proton reservoirs H_{NP}, can be expressed as

$$H_{\mathrm{SD}}=\sum_k(\varepsilon_{k\mathrm{S}}c_{k\mathrm{S}}^\dagger c_{k\mathrm{S}}+\varepsilon_{k\mathrm{D}}c_{k\mathrm{D}}^\dagger c_{k\mathrm{D}}),$$

$$H_{\mathrm{NP}}=\sum_q(\varepsilon_{q\mathrm{N}}d_{q\mathrm{N}}^\dagger d_{q\mathrm{N}}+\varepsilon_{q\mathrm{P}}d_{q\mathrm{P}}^\dagger d_{q\mathrm{P}}). \quad (4)$$

Here, $\varepsilon_{k\mathrm{S}}$ and $\varepsilon_{k\mathrm{D}}$ are the energies of the electrons in the S and D reservoirs and depend on the quasimomentum parameter k. The energies of the protons in the N and P reservoirs $\varepsilon_{q\mathrm{N}}$ and $\varepsilon_{q\mathrm{P}}$ depend on another continuous parameter q.

Electrons in the source and drain reservoirs ($\varsigma=\mathrm{S},\mathrm{D}$) and protons on the negative and positive ($\sigma=\mathrm{N},\mathrm{P}$) sides of the membrane can be characterized by the corresponding Fermi distributions $f_\varsigma(\varepsilon_{k\varsigma})$ and $F_\sigma(\varepsilon_{q\sigma})$

$$f_\varsigma(\varepsilon_{k\varsigma})=\left[\exp\left(\frac{\varepsilon_{k\varsigma}-\mu_\varsigma}{T}\right)+1\right]^{-1},$$

$$F_\sigma(\varepsilon_{q\sigma})=\left[\exp\left(\frac{\varepsilon_{q\sigma}-\mu_\sigma}{T}\right)+1\right]^{-1}. \quad (5)$$

We introduce here the electrochemical potentials μ_σ of the proton reservoirs and the potentials μ_ς for the electron source and drain. The potential μ_S is related to the highest-occupied energy level of the molecular complex S supplying the ETC with electrons, and the potential μ_D plays a similar role for the molecular complex D providing an electron outflow.

Couplings between the electron site 1 (heme b_P) and the source S and between the site 6 (heme b_H) and the electron drain D are determined by the Hamiltonian

$$H_e = -\sum t_{kS}\, c_{kS}^{\dagger}\, a_1 - \sum t_{kD}\, c_{kD}^{\dagger}\, a_6 + \text{H.c.}, \tag{6}$$

with the corresponding transition coefficients t_{kS} and t_{kD}. The similar Hamiltonian describes proton transitions between the shuttle and the proton reservoirs,

$$H_p = -\sum (T_{qN}\, d_{qN}^{\dagger} + T_{qP}\, d_{qP}^{\dagger})(b_7 + b_8) + \text{H.c.} \tag{7}$$

Here, the coefficients T_{qN} and T_{qP}, which are assumed to be the same for both sites 7 and 8, depend on the shuttle position x. The transitions between the redox sites 1, 6, and the electron source S and drain D, as well as between the N and P sides of the membrane and the protonable sites 7, 8 on the shuttle are determined by the energy-independent electron and proton rates [16–20]

$$\gamma_s = 2\pi \sum_k |t_{ks}|^2 \delta(E - \varepsilon_{ks}),$$

$$\Gamma_\sigma = 2\pi \sum_q |T_{q\sigma}|^2\ \delta E - E_{q\sigma}). \tag{8}$$

The proton transition rates Γ_N, Γ_P depend on the distances (either $x+x_0$ or x_0-x) between the shuttle and the N or P sides of the membrane,

$$\Gamma_N = \Gamma_{N0}\left[\exp\left(\frac{x+x_0}{l_p}\right)+1\right]^{-2},$$

$$\Gamma_P = \Gamma_{P0}\left[\exp\left(\frac{x_0-x}{l_p}\right)+1\right]^{-2}, \tag{9}$$

where $x=x(t)$ is the coordinate of the shuttle and l_p is the proton transition length.

The electron tunneling between the redox centers $1,\ldots,6$ is governed by the Hamiltonian H_{tun},

$$H_{tun} = -\Delta_{12}a_1^{\dagger}a_2 - \Delta_{23}a_2^{\dagger}a_3 - \Delta_{24}a_2^{\dagger}a_4 - \Delta_{35}a_3^{\dagger}a_5 - \Delta_{45}a_4^{\dagger}a_5 - \Delta_{56}a_5^{\dagger}a_6 + \text{H.c.} \tag{10}$$

The electrons are transferred between the site 2 located at $x=-x_0$ and the electron-binding sites 3 and 4 on the shuttle. On the opposite side of the membrane at $x=x_0$, the electrons tunnel from the sites 3 and 4 to the site 5. These transfers drastically depend on the shuttle position x. According to quantum mechanics, we can model the position dependence of the tunneling coefficients by the exponential functions,

$$|\Delta_{23}|^2 = |\Delta_{24}|^2 = |\Delta_2|^2 \exp\left(-2\frac{|x+x_0|}{l_e}\right),$$

$$|\Delta_{35}|^2 = |\Delta_{45}|^2 = |\Delta_5|^2 \exp\left(-2\frac{|x-x_0|}{l_e}\right), \tag{11}$$

where l_e is an electron-tunneling length.

B. Environment

The atomic motion of the protein medium has a significant effect on the electron charge transfer between the active sites. Usually (see Refs. [23–25]), the environment is represented as a collection of independent harmonic oscillators. The coupling of these oscillators to electronic degrees of freedom can be described by the Hamiltonian H_{env},

$$H_{env} = \sum_j \frac{p_j^2}{2m_j} + \frac{1}{2}\sum_j m_j\omega_j^2\left(x_j - \sum_{\alpha=1}^{6} x_{j\alpha}n_\alpha - x_{jS}n_S - x_{jD}n_D\right)^2. \tag{12}$$

Here, x_j and p_j are the position and momentum of the j oscillator, having mass m_j and a frequency ω_j. Also, $n_S = \Sigma_k c_{kS}^{\dagger}c_{kS}$ and $n_D = \Sigma_k c_{kD}^{\dagger}c_{kD}$ are the total populations of the source and drain reservoirs; $x_{j\alpha}$, x_{jS}, and x_{jD} is the set of coupling constants between electrons and their surroundings.

Thus, the total Hamiltonian of the system has the form

$$H = H_0 + H_{SD} + H_{NP} + H_e + H_p + H_{tun} + H_{env}. \tag{13}$$

A unitary transformation $H' = U^{\dagger}HU$, with

$$U = \exp\left\{-i\sum_j p_j\left(\sum_\alpha x_{j\alpha}n_\alpha + x_{jS}n_S + x_{jD}n_D\right)\right\}, \tag{14}$$

applied to the Hamiltonian H removes the environment variables $\{x_j\}$ from the Hamiltonian H_{env} and introduces phase shifts into the tunneling Hamiltonian H_{tun},

$$H' = H_0 + H_{SD} + H_{NP} + H_e + H_p + H'_{tun} + \sum_j\left(\frac{p_j^2}{2m_j} + \frac{m_j\omega_j^2x_j^2}{2}\right), \tag{15}$$

where

$$H'_{tun} = -Q_{12}a_1^{\dagger}a_2 - Q_{23}a_2^{\dagger}a_3 - Q_{24}a_2^{\dagger}a_4 - Q_{35}a_3^{\dagger}a_5 - Q_{45}a_4^{\dagger}a_5 - Q_{56}a_5^{\dagger}a_6 + \text{H.c.} \tag{16}$$

is a new tunneling Hamiltonian, and

$$Q_{\alpha\alpha'} = Q_{\alpha'\alpha}^{\dagger} = \Delta_{\alpha\alpha'}\exp\left\{i\sum_j p_j(x_{j\alpha} - x_{j\alpha'})\right\} \tag{17}$$

is a phase shift corresponding to the electron transition from site α' to site α ($\hbar=1$). For simplicity, we neglect here the phase shifts for transitions between the source reservoir and the site 1, $x_{jS}=x_{j1}$, and between the site 6 and the electron drain, $x_{j6}=x_{jD}$, together with shifts related to proton transfers. The electron and proton reservoirs are described by continuous energy spectra. The broadening of the reservoir energy states allows nonresonant transitions, e.g., between site 1 and the source S, thus, reproducing some effects of the corresponding (1-to-S) phase shifts. Recall also that the tunneling rates $\Delta_{\alpha\alpha'}$ for transitions between the sites 2 and 3, 2 and 4, 3 and 5, and 4 and 5 depend on the shuttle position $x(t)$ and—thus—depend on time [see Eq. (11)]. However, this time dependence is much slower than the time variations in environment-induced phase factors.

C. Basis states

To describe all possible occupational configurations of the electron-proton system, we introduce a basis of 256 eigenstates $|\mu\rangle$ of the Hamiltonian $H_0: H_0|\mu\rangle = E_\mu|\mu\rangle$, $\mu = 1, \ldots, 256$, characterized by the energy spectrum E_μ. The basis begins with the vacuum state, where there are no particles on the sites $1, \ldots, 8: |1\rangle = |0_1 0_2 0_3 0_4 0_5 0_6 0_7 0_8\rangle$, and finally ends with the state $|256\rangle$ describing the fully populated system $|256\rangle = |1_1 1_2 1_3 1_4 1_5 1_6 1_7 1_8\rangle$. Here, the notation 0_α (1_α) means that the electron site α is empty (occupied). Similar notations are introduced for the proton sites 7 and 8.

It is of interest that all operators of the system, except the operators of the electron and proton reservoirs, can be expressed in terms of the basic Heisenberg operators $\rho_{\mu\nu} = |\mu\rangle\langle\nu|$, for example,

$$a_\alpha^\dagger a_{\alpha'} = \sum_{\mu\nu} (a_\alpha^\dagger a_{\alpha'})_{\mu\nu} \rho_{\mu\nu},$$

$$a_\alpha = \sum_{\mu\nu} a_{\alpha;\mu\nu} \rho_{\mu\nu}, \quad b_\beta = \sum_{\mu\nu} b_{\beta;\mu\nu} \rho_{\mu\nu}, \tag{18}$$

where $\alpha, \alpha' = 1, \ldots, 6$; $\beta = 7, 8$; and

$$a_{\alpha;\mu\nu} = \langle\mu|a_\alpha|\nu\rangle, \quad b_{\beta;\mu\nu} = \langle\mu|b_\beta|\nu\rangle$$

are the matrix elements of the electron and proton operators in the basis $|\mu\rangle$. The Hamiltonian H_0 has a diagonal form,

$$H_0 = \sum_{\mu=1}^{256} E_\mu \rho_\mu, \tag{19}$$

whereas the tunneling Hamiltonian H_{tun} (we drop hereafter a prime sign) has only off-diagonal elements,

$$H_{\text{tun}} = -\sum_{\mu\nu} \mathcal{A}_{\mu\nu} \rho_{\mu\nu} + \text{H.c.} \tag{20}$$

Here ρ_μ denotes a diagonal operator $\rho_\mu \equiv \rho_{\mu\mu} = |\mu\rangle\langle\mu|$ and $\mathcal{A}_{\mu\nu}$ is a combination of operators, describing the environment,

$$\mathcal{A}_{\mu\nu} = Q_{12}(a_1^\dagger a_2)_{\mu\nu} + Q_{23}(a_2^\dagger a_3)_{\mu\nu} + Q_{24}(a_2^\dagger a_4)_{\mu\nu} + Q_{35}(a_3^\dagger a_5)_{\mu\nu} + Q_{45}(a_4^\dagger a_5)_{\mu\nu} + Q_{56}(a_5^\dagger a_6)_{\mu\nu}. \tag{21}$$

The Hamiltonian H_e, modeling the electron transfer from the source and drain to the sites 1 and 6, and the Hamiltonian H_p, which is responsible for proton transitions between the shuttle and the proton reservoirs, are also expressed in terms of the basis matrix $\rho_{\mu\nu}$,

$$H_e = -\sum_k \sum_{\mu\nu} (t_{k\text{S}} c_{k\text{S}}^\dagger a_{1;\mu\nu} + t_{k\text{D}} c_{k\text{D}}^\dagger a_{6;\mu\nu}) \rho_{\mu\nu} + \text{H.c.}.$$

$$H_p = -\sum_q \sum_{\mu\nu} (T_{q\text{N}} d_{q\text{N}}^\dagger + T_{q\text{P}} d_{q\text{P}}^\dagger)(b_{7;\mu\nu} + b_{8;\mu\nu}) \rho_{\mu\nu} + \text{H.c.} \tag{22}$$

D. Master equation

The average value $\langle\rho_\mu\rangle$ of the operator ρ_μ determines the probability to find the system in the state $|\mu\rangle$. This probability can be found from the Heisenberg equation,

$$\dot{\rho}_\mu = -i[\rho_\mu, H_e + H_p]_- - i[\rho_\mu, H_{\text{tun}}]_-, \tag{23}$$

averaged over the states of reservoirs and over fluctuations of the environment. It is convenient to employ methods of quantum transport theory and the theory of open quantum systems [16–20,26] to derive the set of master equations describing the time evolution of the probability distribution $\langle\rho_\mu\rangle$,

$$\langle\dot{\rho}_\mu\rangle = \sum_\nu (\kappa_{\mu\nu} + \gamma_{\mu\nu})\langle\rho_\nu\rangle - \sum_\nu (\kappa_{\nu\mu} + \gamma_{\nu\mu})\langle\rho_\mu\rangle, \tag{24}$$

where the transition matrix,

$$\kappa_{\mu\nu} = (\kappa_{12})_{\nu\mu} + (\kappa_{23})_{\nu\mu} + (\kappa_{24})_{\nu\mu} + (\kappa_{35})_{\nu\mu} + (\kappa_{45})_{\nu\mu} + (\kappa_{56})_{\nu\mu}, \tag{25}$$

is represented as a sum of Marcus rates $(\kappa_{\alpha\alpha'})_{\nu\mu}$ associated with allowed transitions between the redox states [24,27,28],

$$(\kappa_{\alpha\alpha'})_{\mu\nu} = |\Delta_{\alpha\alpha'}|^2 \sqrt{\frac{\pi}{\lambda_{\alpha\alpha'} T}} [|(a_\alpha^\dagger a_{\alpha'})_{\mu\nu}|^2 + |(a_\alpha^\dagger a_{\alpha'})_{\nu\mu}|^2] \times \exp\left[-\frac{(\omega_{\mu\nu} - \lambda_{\alpha\alpha'})^2}{4\lambda_{\alpha\alpha'} T}\right], \tag{26}$$

where $\omega_{\mu\nu} = E_\mu - E_\nu$, and $\lambda_{\alpha\alpha'}$ is the reorganization energy corresponding to the electron transition between α to α' redox sites [18,20,24]. The relaxation matrix $\gamma_{\mu\nu}$ describes a contribution of transitions between the active sites and the electron and proton reservoirs,

$$\begin{aligned}\gamma_{\mu\nu} = {} & \gamma_\text{S}\{|a_{1;\mu\nu}|^2[1 - f_\text{S}(\omega_{\nu\mu})] + |a_{1;\nu\mu}|^2 f_\text{S}(\omega_{\mu\nu})\} \\ & + \gamma_\text{D}\{|a_{6;\mu\nu}|^2[1 - f_\text{D}(\omega_{\nu\mu})] + |a_{6;\nu\mu}|^2 f_\text{D}(\omega_{\mu\nu})\} \\ & + \Gamma_\text{N}\{(|b_{7;\mu\nu}|^2 + |b_{8;\mu\nu}|^2)[1 - F_\text{N}(\omega_{\nu\mu})] \\ & + (|b_{7;\nu\mu}|^2 + |b_{8;\nu\mu}|^2) F_\text{N}(\omega_{\mu\nu})\} + \Gamma_\text{P}\{(|b_{7;\mu\nu}|^2 + |b_{8;\mu\nu}|^2) \\ & \times [1 - F_\text{P}(\omega_{\nu\mu})] + (|b_{7;\nu\mu}|^2 + |b_{8;\nu\mu}|^2) F_\text{P}(\omega_{\mu\nu})\}.\end{aligned} \tag{27}$$

E. Coulomb energy and redox potential of the shuttle

The electrostatic coupling between electrons and protons traveling together on the menaquinol molecular shuttle is of prime importance for the electron-to-proton energy conversion. For the sake of simplicity and without loss of generality, we describe all electrostatic interactions involved in Eq. (1) by a single electrostatic energy $u_0: u_{37} = u_{38} = u_{47} = u_{48} = u_0$ and $u_{34} = u_{78} = u_0$. It should be noted that the present model tolerates a significant spread (at least 20% and sometimes larger) of the electrostatic parameters. The energy scale u_0 is related to the redox potential E_m of the MQ/MQH_2 couple, which is about −80 meV [10]. To find this relation, we model a process of redox titration of a molecule, which has one electron and one proton-binding sites characterized by the energy levels ε_e and ε_p, respectively.

The electron-binding site is connected to the reservoir of electrons with an electrochemical potential μ_e, whereas the protonable site is coupled to the proton reservoir with an

electrochemical potential μ_p. The energy of the electron-proton Coulomb attraction is determined by the parameter u_0. The goal here is to determine a relation between the electron potential μ_e and the energy scales ε_e and u_0 when the electron-binding site is half-populated. According to the redox titration procedure [29], this value of the "ambient" potential $(\mu_e)_{1/2}$ determines the redox potential of the molecule E_m in the presence of electron-proton electrostatic coupling $E_m=-\mu_{e,1/2}$. As in the case of quinone/quinol molecule, the protonable site should be populated if and only if the electron-binding site is fully occupied. This occurs at the condition

$$\varepsilon_p > \mu_p > \varepsilon_p - u_0.$$

Thus, the average electron $\langle n_e\rangle$ and proton $\langle n_p\rangle$ populations of the molecule are expressed in terms of the Fermi distribution function $f(\varepsilon)$ of the electron reservoir,

$$\langle n_e\rangle = \langle n_p\rangle = \frac{f(\varepsilon_e)}{1+f(\varepsilon_e)-f(\varepsilon_e-u_0)}. \quad (28)$$

The molecule is half-populated with an electron $\langle n_e\rangle=1/2$ and with a proton $\langle n_p\rangle=1/2$ when

$$\mu_{e,1/2} = -E_m = \varepsilon_e - \frac{u_0}{2}. \quad (29)$$

Calculations for a molecule having two electron sites (with energies $\varepsilon_3=\varepsilon_4=\varepsilon_e$) and two proton-binding sites (with the energy levels $\varepsilon_7=\varepsilon_8=\varepsilon_p$) also show the validity of the relation (29) for the case of a single electrostatic parameter u_0.

F. Proton-motive force

The difference of proton electrochemical potentials $\Delta\mu=\mu_P-\mu_N$ defines the transmembrane proton-motive force $\Delta\mu$, consisting of a voltage gradient V and a contribution of the concentration difference ΔpH, between the sides of the membrane [1,2,4],

$$\Delta\mu = V - 2.3(RT/F)\Delta pH. \quad (30)$$

We introduce here the gas constant R and the Faraday constant F. The potentials $\Delta\mu$ and V are measured in meV, whereas temperature T is measured in Kelvin ($k_B=1$). At room temperature $T=298$ K and at the standard gradient of proton concentrations $\Delta pH=-1$, the voltage part of the proton-motive force dominates over the contribution of the concentration gradient $\Delta\mu\simeq V+60$ meV. For example, at $\Delta\mu=200$ meV the voltage difference $V\sim 140$ meV is applied across the membrane. As a consequence of this, the energies ε_α of the redox sites located on the Fdh-N and Nar enzymes are shifted from their original values $\varepsilon_\alpha^{(0)}$,

$$\varepsilon_\alpha = \varepsilon_\alpha^{(0)} + \frac{1}{2}(-1)^\alpha V, \quad (31)$$

where $(\alpha=1,2,5,6)$. We assume here that the voltage drops linearly across the membrane [13], so that the positions of the energy levels of the electron and proton-binding sites on the shuttle are linear functions of the shuttle coordinate x,

$$\varepsilon_3 = \varepsilon_4 = \varepsilon_e^{(0)} - \frac{x}{2x_0}V,$$

$$\varepsilon_7 = \varepsilon_8 = \varepsilon_p^{(0)} + \frac{x}{2x_0}V, \quad (32)$$

Here, $\varepsilon_e^{(0)}$ and $\varepsilon_p^{(0)}$ are the original values of the electron and proton energies of the shuttle.

G. Langevin equation

Within the present model, the Brownian motion of the molecular shuttle [30,31] along a line, which connects the site 2 $(x=-x_0)$ and the site 5 $(x=x_0)$, is governed by the one-dimensional overdamped Langevin equation

$$\zeta\dot{x} = -\frac{dU_c(x)}{dx} - \langle(n_3+n_4-n_7-n_8)^2\rangle\frac{dU_s(x)}{dx} + \xi, \quad (33)$$

where ζ is the drag coefficient of the shuttle in the lipid membrane. The zero-mean valued $\langle\xi\rangle=0$ fluctuation force ξ has Gaussian statistics with the correlation function $\langle\xi(t)\xi(t')\rangle=2\zeta T\delta(t-t')$, proportional to the temperature T of the environment. The diffusion coefficient D of the shuttle is determined by the Einstein relation $D=T/\zeta$. The potential $U_c(x)$,

$$U_c(x) = U_{c0}\left\{1-\left[\exp\left(\frac{x-x_c}{l_c}\right)+1\right]^{-1} + \left[\exp\left(\frac{x+x_c}{l_c}\right)+1\right]^{-1}\right\}, \quad (34)$$

is responsible for the spatial confinement of the menaquinone/menaquinol molecule inside the plasma membrane with the barrier height U_{c0}, the width $2x_c$ $(x_c\geq x_0)$, and the steepness l_c. We also include in Eq. (33) the potential $U_s(x)$ in Eq. (2) hampering the Brownian motion of the charged shuttle across the lipid membrane.

III. PARAMETRIZATION OF THE MODEL

A. Electron-transport chain

Within our model the electron-transport chain begins with the source reservoir S characterized by the chemical potential μ_S, which is related (with an opposite sign) to the redox energy of formate, $\mu_S=420$ meV [6]. The redox potentials of hemes b_P (site 1) and b_C (site 2) located in Fdh-N are not known. We choose the following values $\varepsilon_1^{(0)}=445$ meV and $\varepsilon_2^{(0)}=260$ meV, for the intrinsic energies of sites 1 and 2. Notice that with the transmembrane voltage $V=140$ meV, the energy [see Eq. (31)] of the site 1 $\varepsilon_1=375$ meV is below the potential μ_S, which is a necessary condition for electron transfer from the source reservoir S to the site 1.

The original energy of electron-binding sites on the shuttle $\varepsilon_e^{(0)}$ can be related to the redox potential E_m of the quinone/semiquinone (MQ^-/MQ) couple. It is known [32,33] that the redox energy of the quinone/semiquinone couple is much lower than the potential of the quinone/quinol couple. For example, the potential E_m for the

ubiquinone/ubiquinone (UQ/UQH_2) couple is about +60 mV and the E_m for UQ^-/UQ couple in aqueous solution is on the order of −160 mV [4]. For the redox energy of the MQ^-/MQ couple, we choose a value $E_m=-215$ meV, which is below the known redox energy $E_m=-80$ meV of the MQ/MQH_2 couple. This means that the energy level of the electron-binding sites is placed at $\varepsilon_e^{(0)}=215$ meV. With Eq. (29), we obtain a reasonable estimation for the charging energy of the shuttle,

$$u_0 = 2(\varepsilon_e^{(0)} - \mu_{e,1/2}) = 270 \text{ meV},$$

at $\mu_{e,1/2}=-E_m(MQ/MQH_2)=80$ meV. This value of the charging energy u_0 roughly corresponds to the electrostatic interaction of two charges located on the opposite sides of the menaquinone molecule [34] at a distance ~0.6 nm provided that the dielectric constant $\epsilon \sim 9$.

We note that at the voltage difference $V=140$ meV, the energy level of the site 2, $\varepsilon_2=330$ meV, is higher than the level $\varepsilon_e^{(0)}+V/2=285$ meV of an electron on the shuttle located at the N side. Because of this, electrons can be transferred from site 2 to the menaquinone followed by the proton uptake from the N side of the membrane.

The unloading of the fully populated shuttle occurs at the P side provided the energy of the electrons on the shuttle $\varepsilon_e^{(0)}-u_0-V/2=-125$ meV exceeds the energy ε_5 of the site 5. Here, for $V=140$ meV, we choose sufficiently low values $\varepsilon_5=-170$ meV and $\varepsilon_6=-215$ meV, for energy levels of the redox sites 5 and 6 belonging to the second half of the redox loop, whereas the original values are $\varepsilon_5^{(0)}=-100$ meV and $\varepsilon_6^{(0)}=-285$ meV. The corresponding redox potentials of these sites differ from the measured redox levels [10] of heme b_L: $E_m \sim 20$ mV (site 5) and heme b_H: $E_m \sim 120$ mV (site 6). It is known, however, that the redox potentials obtained as a result of equilibrium redox titrations are not always applicable for a description of the electron transfer in enzymes, in particular, because of cooperativity between the redox centers [10]. This cooperativity can be induced, e.g., by electrostatic couplings between the redox sites 1 and 2: $u_{12}=20$ meV, and between the sites 5 and 6: $u_{56}=20$ meV. In the present model, the electron-transport chain terminates at the drain reservoir characterized (at $V=140$ meV) by the energy scale $\mu_D=-260$ meV, which exceeds the energy $-E_m=-420$ meV of electrons at the site of nitrate-to-nitrite reduction [10].

B. Proton pathway

Protons are loaded on the shuttle at the N side ($x \sim -x_0$) provided that the shuttle is populated at least with one electron. This condition can be met at $\varepsilon_p^{(0)}=u_0/2$ when the energy $u_0/2-V/2=65$ meV of a proton on the shuttle located at $x=-x_0$ is higher than the potential μ_N, whereas the proton energy level $-u_0/2-V/2=-205$ meV of the shuttle populated with electrons is below μ_N. We take into account electron-electron and proton-proton Coulomb repulsions on the shuttle and assume that $V=140$ meV, so that the total transmembrane proton-motive force $\Delta\mu=\mu_P-\mu_N$ is about 200 meV [35] with $\mu_N=-100$ meV and $\mu_P=+100$ meV.

Unloading of protons, which occurs at the P side of the membrane ($x \sim x_0$) is preceded by the electron transfer to the site 5. Then, the proton energy goes up, to the level $\varepsilon_p^{(0)}+V/2=205$ meV, exceeding the potential μ_P. It should be noted that the present model is robust to pronounced variations ($\Delta\varepsilon \sim 50$ meV) of electron and proton energy levels (see Fig. 3 later on).

C. Other parameters

It is known [36] that electrons can be transferred between the redox centers in a nanosecond range. The proton transfer mediated by the hydrogen-bonded chains can occur in nanoseconds as well [37,38]. In view of these findings, we choose the following parameters controlling electron and proton transitions between the reservoirs and the active sites: $\gamma_S=\gamma_D=0.5/\text{ns}$, $\Gamma_N=\Gamma_P=0.05/\text{ns}$. We assume that all allowed electron transitions between the redox sites are determined by the same energy scale $\Delta_{\alpha\alpha'}=8$ μeV. For the transition lengths l_e and l_p involved in Eqs. (9) and (11), we have the values $l_e=0.25$ nm and $l_p=0.25$ nm.

The reaction of the environment is described by the set of reorganization energies $\lambda_{\alpha\alpha'}$ [18,20,24], which are also assumed to be the same for every pair $\alpha,\alpha': \lambda_{\alpha\alpha'}=\lambda=100$ meV. A similar value of the reorganization energy has been observed in cytochrome *c* oxidase [39].

The Brownian motion of the shuttle is characterized by the diffusion and drag coefficients D and ζ. For the diffusion coefficient, we take the value $D \sim 3\times 10^{-12}$ m^2/s, measured in Refs. [40,41] for ubiquinone ($T=298$ K). The drag coefficient ζ can be found from the Einstein relation $\zeta=T/D=1.37$ nN s/m. The potential barrier $U_s(x)$ in Eq. (2), which impedes the diffusion of the charged shuttle, is characterized by the energy penalty $U_{s0}=770$ meV, steepness $l_s=0.05$ nm, and half-width $x_s=1.7$ nm. For the potential $U_c(x)$ in Eq. (34), keeping the shuttle inside the membrane, we choose the height $U_{c0}=500$ meV, steepness $l_c=0.1$ nm, and half-width $x_c=2.7$ nm. The redox sites are located at $x_0=\pm 2$ nm. On average, the shuttle travels a distance $2x_0$ between sites 2 and 5 in a time $\Delta t=(2x_0)^2/(2D) \sim 2.7$ μs, which is much longer than the time scales for electron and proton transitions to and from the shuttle.

IV. RESULTS

To quantitatively describe the kinetics of electron and proton transfers across the membrane, we numerically solve the system of master equation (24) together with the Langevin equation (33) for a parameter regime, which provides a robust and efficient proton-motive force generation, and also roughly corresponds to the menaquinone/menaquinol molecule randomly moving inside the bacterial plasma membrane. It should be noted that the present model allows significant variations (~20% and sometimes higher) of the parameter values.

In Fig. 2, we present the time evolution of the electron and proton translocation process at $T=298$ K, $\Delta\mu=200$ meV, and $V=140$ meV. The shuttle starts its motion at $x=x_0$ [Fig. 2(a)] and after that diffuses between the membrane borders (shown by two dashed red lines at $x=\pm 2$ nm). The total electron population $n_e=\langle n_3\rangle+\langle n_4\rangle$ (con-

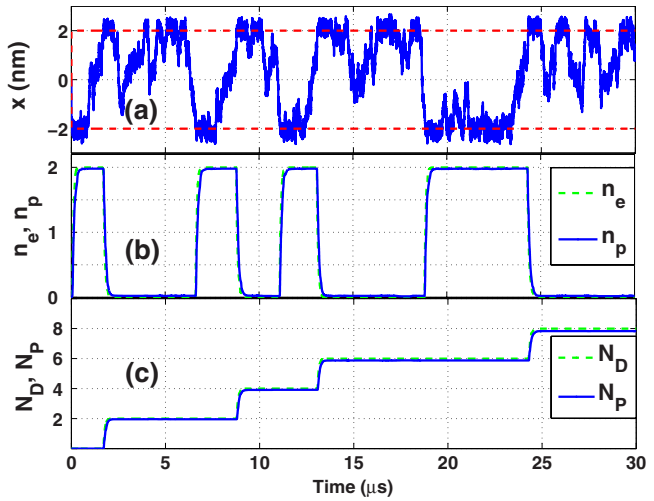

FIG. 2. (Color online) (a) Time dependence of the position x (in nm) (blue continuous curve) of the shuttle, diffusing between the walls of the plasma membrane located at $x=\pm x_0$ (two red dashed horizontal lines), where $x_0=2$ nm; (b) the total proton ($n_p=\langle n_7\rangle+\langle n_8\rangle$, blue continuous curve) and electron ($n_e=\langle n_3\rangle+\langle n_4\rangle$, green dashed curve) populations of the shuttle versus time (in μs); (c) the number of transferred protons (N_P, blue continuous curve) and the number of translocated electrons (N_D, green dashed curve) versus time at $V=140$ meV, $\Delta\mu=200$ meV, and at $T=298$ K. Notice that the shuttle is loaded near the N side of the membrane at $x\approx -x_0$ and unloaded at the P side at $x\approx +x_0$. It follows from (c) that the process of shuttle unloading is accompanied by a stepwise increase in the number of protons N_P translocated to the P side of the membrane and the number of electrons N_D transferred to the site 5 and, finally, to the drain.

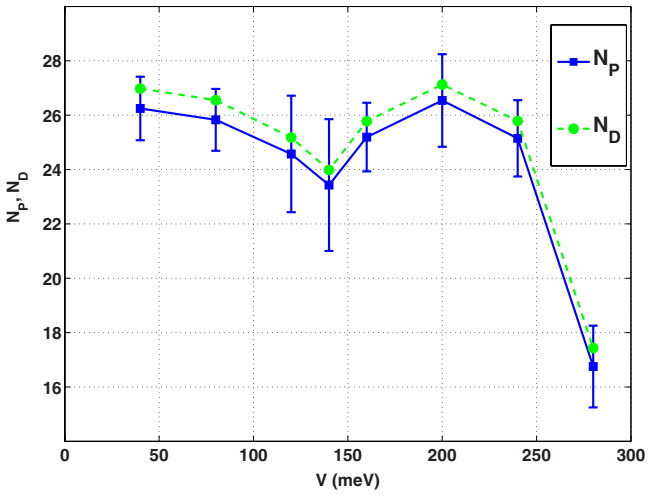

FIG. 3. (Color online) The number of protons N_P (blue continuous line) translocated energetically uphill, from the N side to the P side of the membrane, and the number of electrons N_D (green dashed curve) transferred from the site 2 on the Fdh-N enzyme to the site 5 belonging to the Nar enzyme, as functions of the transmembrane voltage V at $T=298$ K. In Figs. 3 and 4, the results are averaged over ten realizations. Each realization has a time span of 100 μs. Error bars (standard deviations) are shown for the number N_P of translocated protons.

tinuous blue line) and the total proton population $n_p=\langle n_7\rangle+\langle n_8\rangle$ (dashed green line) of the shuttle are shown in Fig. 2(b). The electron sites 3 and 4 are populated and depopulated in concert: $\langle n_3\rangle=\langle n_4\rangle=n_e/2$. The same relation takes place for the proton sites 7 and 8: $\langle n_7\rangle=\langle n_8\rangle=n_p/2$. The populations are averaged over the states of electron and proton reservoirs as well as over the state of the environment. No averaging over fluctuations of the random force $\xi(t)$ in Eq. (33) has been performed in Fig. 2.

The total number of protons N_P (dashed green line) transferred by the shuttle from the N to the P side of the membrane, and the total number of electrons N_D (continuous blue line) translocated from the redox site 2 to the site 5, and, finally, to the electron drain D are shown in Fig. 2(c). At the beginning of the process ($t\sim 0$, $x\sim -x_0$), the shuttle is rapidly populated with two electrons ($n_e=2$) and with two protons ($n_p=2$) taken from the N side of the membrane ($\mu_N=-100$ meV). The fully loaded shuttle diffuses and eventually reaches (at $t\sim 2$ μs) the opposite side, where the electrons are transferred to the redox site 5 ($N_D=2$), and two protons ($N_P=2$) are translocated energetically uphill to the P side of the membrane ($\mu_P=100$ meV). Accumulation of protons on the positive side of the membrane results in a generation of the proton-motive force. The empty and neutral quinone molecule diffuses back to the N side of the membrane [Fig. 2(a)] and the process starts again. Notice that as a consequence of the stochastic nature of the process, the proton population n_p can be a little bit smaller than the electron population n_e of the shuttle [see Fig. 2(b)]. The resulting tiny charge makes more difficult for the shuttle to cross the potential barrier $U_s(x)$ in Eq. (2).

It is evident from Figs. 3 and 4 that the physical mechanism of the proton-motive force generation described above tolerates significant variations in system parameters such as the transmembrane voltage V and temperature T. In Fig. 3 we show the number of protons N_P translocated across the mem-

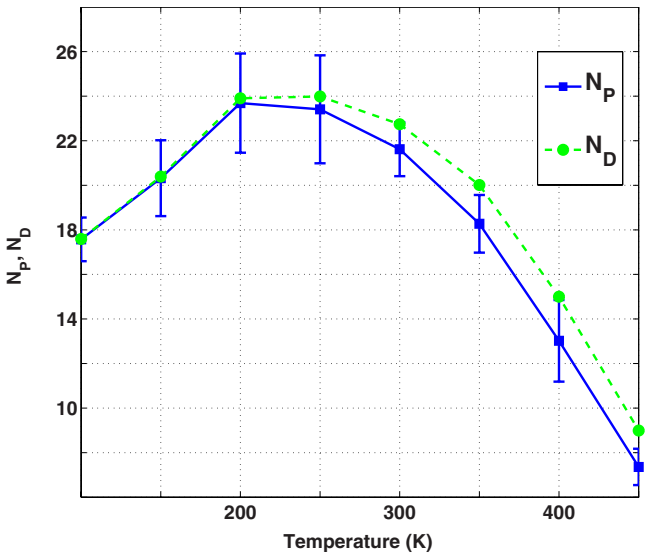

FIG. 4. (Color online) Temperature dependence of the numbers of protons N_P (blue continuous curve, with error bars) and electrons N_D (green dashed curve) transported by the shuttle at the transmembrane voltage $V=140$ meV.

brane and the number of electrons N_D transferred from the site 2 to the site 5 as functions of the transmembrane voltage V at $T=298$ K. Each point in Figs. 3 and 4 is a result of averaging over 10 realizations. Every realization has a duration of 100 μs. We calculate the standard deviations for the number N_P of transferred protons $\sigma_P=\sqrt{\langle N_P^2\rangle-\langle N_P\rangle^2}$ and show these deviations as the error bars in Figs. 3 and 4. The uncertainty σ_D in the number N_D of translocated electrons is close to the value of σ_P. We choose here a symmetric configuration of the proton electrochemical potentials,

$$\mu_P=-\mu_N=\frac{1}{2}\left(V+60\times\frac{T}{298}\right), \tag{35}$$

where the potentials μ_N, μ_P, and the voltage V are measured in meV, and the temperature T is measured in Kelvin.

It follows from Fig. 3 that this redox loop is able to translocate more than 240 protons in one millisecond against the transmembrane voltage $V\sim 200$ meV, which corresponds to the proton-motive force $\Delta\mu\sim 260$ meV. In this case (when $N_P\simeq 265$, $N_D\simeq 270$, $\mu_P=-\mu_N=130$ meV, $\mu_S=420$ meV, and $\mu_D=-260$ meV), the *thermodynamic efficiency* η of the energetically uphill proton translocation,

$$\eta=\frac{N_P}{N_D}\frac{\mu_P-\mu_N}{\mu_S-\mu_D}, \tag{36}$$

reaches the value $\eta\simeq 37\%$.

We note that despite the dielectric penalty of 770 meV for a charged shuttle, the average number of transferred electrons N_D slightly exceeds the number of protons N_P. Interestingly, both numbers N_P and N_D have small dips at $V=140$ meV. With increasing the transmembrane voltage $V\geq 280$ meV, the electron transport from the site 1 ($\varepsilon_1=305$) to the site 2 ($\varepsilon_2=400$) and from the site 5 ($\varepsilon_5=-240$) to the site 6 ($\varepsilon_6=-145$, all energies in meV) become energetically unfavorable. As a result of this, the numbers of electrons N_D and protons N_P translocated across the membrane drop significantly at high voltages.

The temperature dependence of the average numbers of protons N_P and electrons N_D conveyed by the shuttle is presented in Fig. 4 for $V=140$ meV. The system demonstrates stable performance with $N_P\sim 220$ protons/ms in a window of temperatures from 250 K up to 350 K. The initial increase in N_P and N_D with temperature is probably due to the fact that in a warmer environment the shuttle travels more frequently between the sides of the membrane transferring more electrons and more protons. Loading (unloading) the shuttle with protons follows its loading (unloading) with electrons. At high temperatures, menaquinone spends less time in the loading zone (at $x\sim -x_0$) and protons have less opportunity to populate the shuttle. Therefore, the gap between the numbers of transferred protons and electrons widens with increasing temperature. This means that at high temperatures, the shuttle has more chances to carry a charge, which obstructs the shuttle's diffusion across the membrane. Besides that, at sufficiently high temperatures electrons have not enough time to be loaded on the shuttle. A combination of these two features results in the high-temperature decline of electron and proton flows shown in Fig. 4.

V. CONCLUSIONS

Using a simple kinetic model, we have examined the process of proton-motive force generation across the bacterial plasma membrane. This model is applied to the redox loop mechanism of the nitrate respiration in *E. coli*. This approach includes two redox sites in the first half of the redox loop, two redox sites in the second half, and the Brownian shuttle diffusing between the N and P sides of the membrane. We show that the Coulomb attraction between electrons and protons traveling on the shuttle plays an essential role in the energetically uphill proton translocation from the N side to the P side of the membrane and, thus, in the proton-motive force generation. We have derived and numerically solved a set of master equations, which quantitatively describes the process of loading and unloading the shuttle with electrons and protons, along with a stochastic Langevin equation for the shuttle position. Our model is able to explain the generation of the proton-motive force up to 300 meV in the physiologically relevant range of temperatures from 250 to 350 K with a peak thermodynamic efficiency of about 37%. A sequence of electron and proton transport events and main characteristics of the redox loop mechanism calculated in the present paper can be measured in future experiments aimed on a kinetic analysis of the nitrate respiration process in bacteria.

ACKNOWLEDGMENTS

This work was supported in part by the National Security Agency (NSA), Laboratory of Physical Science (LPS), Army Research Office (ARO), and the National Science Foundation (NSF) under Grant No. EIA-0130383. S.E.S. acknowledges support from the EPSRC via Grant No. EP/D072581/1.

[1] B. Alberts, A. Johnson, J. Lewis, M. Raff, K. Roberts, and P. Walter, *Molecular Biology of the Cell* (Garland Science, New York, 2002), Chap. 14.
[2] V. P. Skulachev, *Membrane Bioenergetics* (Springer-Verlag, Berlin, 1988).
[3] R. B. Gennis, in *Biophysical and Structural Aspects of Bioenergetics*, edited by M. Wikström (RSC, Cambridge, 2005).
[4] D. G. Nicholls and S. J. Ferguson, *Bioenergetics 2* (Academic Press, London, 1992).
[5] P. Mitchell, J. Theor. Biol. **62**, 327 (1976).
[6] M. Jormakka, S. Törnroth, B. Byrne, and S. Iwata, Science **295**, 1863 (2002).
[7] M. G. Bertero, R. A. Rothery, M. Palak, C. Hou, D. Lim, F. Blasco, J. H. Weiner, and N. C. Strynadka, Nat. Struct. Biol. **10**, 681 (2003).
[8] D. Richardson and G. Sawers, Science **295**, 1842 (2002).

[9] M. Jormakka, B. Byrne, and S. Iwata, FEBS Lett. **545**, 25 (2003).
[10] F. Blasco, B. Guigliarelli, A. Magalon, M. Asso, G. Giordano, and R. A. Rothery, Cell. Mol. Life Sci. **58**, 179 (2001).
[11] M. L. Verkhovskaya, N. Belevich, L. Euro, M. Wikström, and M. I. Verkhovsky, Proc. Natl. Acad. Sci. U.S.A. **105**, 3763 (2008).
[12] I. Belevich, D. A. Bloch, N. Belevich, M. Wikström, and M. I. Verkhovsky, Proc. Natl. Acad. Sci. U.S.A. **104**, 2685 (2007).
[13] Y. C. Kim, M. Wikström, and G. Hummer, Proc. Natl. Acad. Sci. U.S.A. **104**, 2169 (2007).
[14] R. Sugitani, E. S. Medvedev, and A. A. Stuchebrukhov, Biochim. Biophys. Acta **1777**, 1129 (2008).
[15] A. M. Ferreira and D. Bashford, J. Am. Chem. Soc. **128**, 16778 (2006).
[16] N. S. Wingreen, A.-P. Jauho, and Y. Meir, Phys. Rev. B **48**, 8487 (1993).
[17] D. Weinmann, W. Häusler, and B. Kramer, Phys. Rev. Lett. **74**, 984 (1995).
[18] A. Yu. Smirnov, L. G. Mourokh, and F. Nori, Phys. Rev. E **77**, 011919 (2008).
[19] A. Yu. Smirnov, S. Savel'ev, L. G. Mourokh, and F. Nori, Phys. Rev. E **78**, 031921 (2008).
[20] A. Yu. Smirnov, L. G. Mourokh, and F. Nori, J. Chem. Phys. **130**, 235105 (2009).
[21] M. Mohseni, P. Rebentrost, S. Lloyd, and A. Aspuru-Guzik, J. Chem. Phys. **129**, 174106 (2008).
[22] A. Y. Mulkidjanian, Biochim. Biophys. Acta **1757**, 415 (2006).
[23] A. Garg, J. N. Onuchic, and V. Ambegaokar, J. Chem. Phys. **83**, 4491 (1985).
[24] D. A. Cherepanov, L. I. Krishtalik, and A. Y. Mulkidjanian, Biophys. J. **80**, 1033 (2001).
[25] U. Weiss, *Quantum Dissipative Systems* (World Scientific, Singapore, 2008).
[26] G. F. Efremov and A. Yu. Smirnov, Sov. Phys. JETP **53**, 547 (1981).
[27] R. A. Marcus, J. Chem. Phys. **24**, 966 (1956).
[28] R. A. Marcus and N. Sutin, Biochim. Biophys. Acta **811**, 265 (1985).
[29] L. Euro, D. A. Bloch, M. Wikström, M. I. Verkhovsky, and M. Verkhovskaya, Biochemistry **47**, 3185 (2008).
[30] P. Hänggi, F. Marchesoni, and F. Nori, Ann. Phys. **14**, 51 (2005).
[31] R. F. Fox, Phys. Rev. E **57**, 2177 (1998).
[32] R. C. Prince, P. L. Dutton, and J. M. Bruce, FEBS Lett. **160**, 273 (1983).
[33] A. Osyczka, C. C. Moser, and P. L. Dutton, Trends Biochem. Sci. **30**, 176 (2005).
[34] E. Maklashina, P. Hellwig, R. A. Rothery, V. Kotlyar, Y. Sher, J. H. Weiner, and G. Cecchini, J. Biol. Chem. **281**, 26655 (2006).
[35] J. Simon, R. J. M. van Spanning, and D. J. Richardson, Biochim. Biophys. Acta **1777**, 1480 (2008).
[36] E. Pilet, A. Jasaitis, U. Liebl, and M. H. Vos, Proc. Natl. Acad. Sci. U.S.A. **101**, 16198 (2004).
[37] J. F. Nagle and H. J. Morowitz, Proc. Natl. Acad. Sci. U.S.A. **75**, 298 (1978).
[38] F. Bartl, G. Deckers-Hebestreit, K. Altendorf, and G. Zundel, Biophys. J. **68**, 104 (1995).
[39] A. Jasaitis, F. Rapaport, E. Pilet, U. Liebl, and M. H. Vos, Proc. Natl. Acad. Sci. U.S.A. **102**, 10882 (2005).
[40] B. Chazotte, E.-S. Wu, and C. R. Hackenbrock, Biochim. Biophys. Acta **1058**, 400 (1991).
[41] D. Marchal, W. Boireau, J. M. Laval, J. Moiroux, and C. Bourdillon, Biophys. J. **74**, 1937 (1998).